High temperature instrumented microindentation. Applications to thermal barrier coatings constituent materials.

Bruno Passilly, Pascale Kanoute, Francois-Henri Leroy, Remy Mevrel

High temperature instrumented microindentation. Applications to thermal barrier coatings constituent materials.

Journal:	*Philosophical Magazine & Philosophical Magazine Letters*
Manuscript ID:	TPHM-05-Nov-0482.R2
Journal Selection:	Philosophical Magazine
Date Submitted by the Author:	17-Mar-2006
Complete List of Authors:	PASSILLY, Bruno; ONERA, DMSC KANOUTE, Pascale; ONERA, DMSE LEROY, Francois-Henri; ONERA, DMSC MEVREL, Remy; ONERA, DMMP
Keywords:	FEM, high-temperature materials, indentation testing, intermetallic compounds, thermal barrier coatings
Keywords (user supplied):	

High temperature instrumented microindentation. Applications to thermal barrier coatings constituent materials

B. PASSILLY[1], P. KANOUTE[b], F.-H. LEROY[a], R. MÉVREL[c *]
[a]*ONERA – DMSC, BP 72, 92322 Châtillon Cedex – Tél +33 1 4673 4554 (bruno.passilly@onera.fr)*
[b]*ONERA – DMSE,* [c]*ONERA – DMMP*

ABSTRACT

An original instrumented microindenter capable of testing materials up to 1000°C in an inert atmosphere has been developed. After exposing the principle and its characteristics, the possibilities of the techniques are illustrated with tests on NiAl(Pt) materials representative of the bondcoats of thermal barrier coatings.
A modelling approach based on FEM calculations has been developed, which enables, by solving the inverse problem, to identify the variables of the constitutive law of the materials tested. Confrontation of results thus obtained with published data when available shows a satisfactory agreement.
This experimental technique combined with the modelling approach opens up a new way to determine the constitutive behaviour law of materials at a local scale and in a large range of temperature.

Keywords: Instrumented indentation, Intermetallic compound, Hot hardness, High temperature testing, Thermal barrier coating, FEM

1. Introduction

Instrumented microindentation techniques have been generally developed for room temperature tests. [1]. From the load-displacement curves, it is possible to derive hardness, Young's modulus [2,3] and, through the use of recently proposed approaches, the elastoplastic behaviour law of a material [4,5]. In some cases, it might be most interesting to be able to derive, with this technique, the local mechanical properties at high temperature. Thus, in the case of thermal barrier coatings (TBC), which are multilayer systems [6,7] protecting turbine blades, it is reckoned that the mechanical behaviour of the bondcoat (thickness around 50 µm), constituted of a β-NiAl(Pt) alloy plays a crucial role in the mechanical integrity of the system when thermally cycled [8]. The composition and the microstructure of this bondcoat evolves during service at high temperature, due to oxidation and interdiffusion phenomena and it would be difficult and fastidious to test bulk specimens made of the material constituting the bondcoat. To characterize the high temperature mechanical properties of such systems, some groups [9] have developed mechanical tests on microsamples machined out of thermal barrier coatings, with however, rather tedious practical difficulties. In principle, high temperature instrumented microindentation appears as a technique particularly suitable for the study of such systems. And more generally, one could find an interest for extracting local

* Corresponding author. Email : remy.mevrel@onera.fr

mechanical properties (coatings, individual phases in multiphase materials) or simply mechanical properties of materials at an early stage of research and development.

High temperature indentation has been used by several groups to characterize the creep behaviour of various materials (for a review on impression creep, see for example [10]). Pioneering works by Mulhearn et al. [11], Atkins et al. [12] have pointed out several pitfalls that may underlie the interpretation of data obtained from high temperature indentation tests, in particular the fact that, for a growing plastic zone during an indentation test, applying a steady-state creep equation may not be the most appropriate type of creep relation and a transient law might in some cases be more justified. However, more recently several studies have shown that creep indentation data can be analysed in various cases with a steady-state power law creep equation [13-15]. Sargent and Ashby [13] could thus analyse the creep indentation data of several ceramics and metals for indentation temperature above 0.5 Tm (Tm being the melting point). For low test temperatures, such an analysis may no longer be valid as the deformation mechanisms are outside the power-law regime [16]. Doerner et al. [15] have shown that it is possible to derive creep laws from indentation tests, which are comparable to the laws obtained with conventional uniaxial tests. However, these tests remain macroscopic (indent dimensions are of the order of 1 mm or more) and they would not be suited for studying systems having small dimensions or for testing local properties.

High temperature instrumented microindentation has been employed by several groups to determine Young's modulus. One can mention for example the recent measures of the Young's modulus of a superalloy (CMSX-4) up to 800°C with a microindenter developed by [17]. Young's modulus had been measured by Kim et al. [18] up to 900°C by a similar technique on a porous ceramic coating. Finally, Beake et al. [19, 20] report nanoindentation results up to 400°C and 500°C. However, it does not seem that this technique has been used, up to now to derive a complete elasto-visco-plastic law at high temperature.

In the next part, the instrumented microindenter is described together with the experimental details concerning the materials studied. Then we illustrate the possibilities of the technique by exposing results obtained on NiAl(Pt) alloys whose compositions are representative of materials constituting bondcoats of thermal barrier coatings.

2. Experimental details

2.1 High temperature instrumented microindenter

The configuration and a view of the equipment are shown in figure 1. It comprises a vacuum chamber containing two translation tables (along horizontal X and Y axis) on which the load sensor, the sample holder, the sample and a furnace are fixed. Both translation tables (displacement resolution better than 1 micrometer) can displace the sample from under a microscope to under the indenter.

The microscope, equipped with a camera, enables to locate the points of interest and measure the indentation dimensions at the test temperature. This setup is fixed on a translation table motorised along the vertical Z axis to focus on the sample surface. An autofocus system can link the image acquisition to the Z translation table movement.

The chamber, the portholes, the translation tables and the sensors are cooled with flowing water. A primary vacuum (5.10^{-2} Pa) can be obtained with a Roots pumping system associated with a turbomolecular pump. Pure argon (Argon C, 3ppm O_2, 3ppm H_2O) is introduced inside the chamber to maintain a neutral atmosphere during the high temperature tests.

The indenter and the sample can be heated up to 1000°C by small furnaces regulated at ± 2°C of the set temperature. Typical dimensions of the sample are 10mm*4mm*5mm.

The load is measured with strain gage sensors. The maximum load is 3N and typical loading rates are 10^{-3} N.s^{-1}. The displacements are measured by using a differential capacitive technology.

The load-displacement curves are obtained with a feedback control either on the load or on the displacement signal. The control on the load provides a feedback to reach the desired value directly on the piezoelectric translation table which increments the indenter displacement according to a convergent series. This method enables to generate a variety of test conditions: single or repeated load/unload cycles, constant load during a given period, etc.

'[Insert Figure 1 about here]'

To avoid any thermal drift on the displacement and load sensors, the measurement cell is thermally stabilised with flowing water. Tests done on a ceramic material which is not sensitive to creep up to 900°C, revealed no drift effect in the results.

2.2 Materials

β-NiAl(Pt) alloy ingots were prepared by arc melting of pure Ni, Al and Pt powders. They were remelted at least five times in high-purity argon atmosphere, using titanium getter. Cylinders of 10 mm diameter were machined out of the ingots and annealed at 1300°C for 25 h in argon (enwrapped in niobium foils), to homogenize their compositions. Specimens were sectioned out of these cylinders and sections were ground with SiC abrasive papers and successively polished with 6, 2 and 0.25 µm diamond pastes, and finally rinsed with acetone in an ultrasonic cleaner and dried.

The intermetallic NiAl(Pt) compounds have a B2 crystallographic structure (melting point of $Ni_{50}Al_{50}$: 1610K) and the ingots used in this study had a grain size of several hundreds of micrometers, so the influence of neighbouring grains can be considered negligible.

2.3 Observation and analysis

The compositions of the alloys were determined by EDS analysis in a scanning electron microscope. Some indentation profiles were determined by atomic force microscopy.

3. Results and discussion

3.1 Simplified approach of creep properties of NiAl(Pt)

Instrumented microindentation tests have been performed on a $Ni_{40}Al_{45}Pt_{15}$ alloy with a loading rate of 0.004 N/s with holding time of 1600s at the maximum load (0,7 N). For each temperature, between 700°C and 800°C, 3 tests have been done. Figure 2 displays typical (uncorrected) load-displacement curves and figure 3 shows the variations in time of the displacements while the load is maintained at its maximum.

'[Insert Figure 2 about here]' '[Insert Figure 3 about here]'

To interpret these variations, it is possible to apply relatively simple approaches developed to characterize the deformation of materials indented at high temperature [13,14].

The steady-creep rate for NiAl compounds can be characterized, above 0.5Tm, by a power-law creep equation [21] of the form:

$$\dot{\varepsilon} = \dot{\varepsilon}_0 (\sigma / \sigma_0)^n \qquad (1)$$

where $\dot{\varepsilon}$ is the strain rate, σ the stress, σ_0 a constant and $\dot{\varepsilon}_0 = k.\exp(-Q/RT)$ in which Q is an activation energy, T the temperature, R the perfect gas constant and the pre-exponential factor k is a constant. Given such a law, it can be shown that the displacement of the indenter during a creep test can be described with the following expression, derived by [13] form a dimensional analysis (and slightly modified to take into account an initial transient regime):

$$u = \left[(u_0)^{n/2} + B.n.(t - t_0) \right]^{n/2} \qquad (2)$$

where u_0 is the value of the displacement corresponding to time t_0, after which the deformation can be considered as stationary creep; parameter B depends on the temperature according to the equation:

$$B = B_1.\exp(-Q/R.T) \qquad (3)$$

By fitting the displacement u given by equation (2) to the experimental data (figure 3), we find an exponent value n between 3.5 and 4.2. According to the variation in temperature of B, given in figure 4, we find an activation energy of 297 ± 25 kJ/mole. These values are of the same order as the values reported by Noebe et al. [21] in their review paper on NiAl. For temperatures between 1023K and 1400K, the values reported for the exponent n are between 4 and 7 and the activation energy is in the range between 293 – 350 kJ/mole. According to Noebe [21], these values tend to show that at these temperatures, the creep is climb-controlled.

'[Insert Figure 4 about here]'

These encouraging results indicate that such a simplified approach might be used to estimate rapidly the creep behaviour of such materials. However, more work is needed to appreciate to what extent the method can be generalized. A more complex and rigorous mechanical approach has been engaged, which is exposed in the following part.

3.2 Simulation based on FEM calculations, identification of constitutive models

The objective of the modelling work engaged is to extract the evolution in temperature of the mechanical properties of these bondcoat materials using a data reduction procedure based on numerical optimisation. For that, modelling the indentation test by finite element analysis has been undertaken using the Zebulon code developed by Onera and by the School of Mines, Paris. In this study the three-dimensional indentation induced via Vickers geometry was approximated with an axisymmetric model, choosing the apex angle θ (70.3°) such that the projected area/depth of the two-dimensional cone and that of the Vickers indenter are identical. In the finite element calculations, the indenter was modelled either as a diamond or a ruby body and the contact as frictionless. Moreover, the calculations were performed within the large deformation assumption. The finite element model enables to finely describe the elasto-viscoplastic behaviour of the indented material and several constitutive equations can be introduced in the model. The models used in the identification process are consistent with the unified viscoplastic formalism developed by Chaboche et al. [22, 23] which allows a unified description of yielding, creep, stress relaxation, and a variety of other mechanical effects, such as Bauschinger effects and time recovery. It uses the superposition of several isotropic and kinematic hardening variables, each of them satisfying an evolution equation that incorporates strain hardening, dynamic recovery and thermal recovery. The

corresponding constitutive equations are listed in Table 1. In the present paper, isotropic hardening and thermal recovery are not considered.

'[Insert Table 1 about here]'

The strain is assumed to be composed of elastic ε_e and inelastic ε_p parts as written in equation (4). An elastic domain is assumed, written in the stress space by means of the thermodynamic forces associated with the internal variables, as in equation (5). For an isotropic material, the distance in the stress space is formulated using the Von Mises criterion given by equation (6) where $\boldsymbol{\sigma}_y$ is the true elasticity limit. In this expression, the back stress tensor X associated to variables α_i gives the position of the elastic domain. σ' and X' are the deviators of the stress and of the back stress tensors respectively. The kinematic hardening results from the superposition of several independent variables α_i (equation (7)) which evolution laws are given by the combination of a static recovery term and a dynamic recovery term, as written in equation (8) where C_i, D_i are material parameters. The MacCauley brackets (in equation (10)) are defined by $< u >= u$ if $u \geq 0$ or $< u >= 0$ if $u \leq 0$. Such evolution equations reproduce in a tensorial macroscopic writing the athermal dislocation-based interaction mechanisms including short and long range interactions. The viscoplastic flow rule is taken as a power function of the plastic strain rate and described by equations (9) and (10). Exponent n plays an analogous role to creep exponent in equation (1) and σ_d is a drag parameter (that could be affected by isotropic hardening effects). In principle σ_y, σ_d, C_i and exponent n are temperature dependent parameters. As usual the norms of the stress and of the plastic strain are chosen in order to recover the corresponding absolute values of the σ_{11} and $\dot{\varepsilon}_{p11}$ components in the particular case of uniaxial conditions (Lemaitre and Chaboche) [24].

3.2.1. Identification of the room temperature behaviour of TBC constituents. The first application was on a bulk $Ni_{60}Al_{35}Pt_5$ sample whose composition is representative of a bondcoat after prolonged oxidation. The identification was first performed for properties at room temperature where the viscous effects are negligible. The optimisation procedure involves a quadratic descent method (Levenberg-Marquardt). Inverse simplified methods of the literature are also used to start efficiently the iterative optimisation given the lengthy computational time of a single iteration (FE modelling in large deformations with contact conditions). The identification comprises on the one hand determining the parameters of these elasto-viscoplastic constitutive equations based on the superposition of isotropic and kinematic hardening variables, and on the other hand characterizing the curve of the equivalent behaviour. The identification obtained, reported in figure 5, provides a good description of the cyclic indentation test (2 cycles).

3.2.2. Identification of the variations in temperature of the behaviour of TBC constituents. Identification at high temperature is performed using the assumption that all the plastic behaviour properties are globally reduced by the increase of temperature in the same way.
A multi-objective optimisation procedure is used to characterize the plasticity parameters in parallel with the viscosity parameters n and σ_d using indentation tests with dwell time and variable loading rates. Comparisons between experimental and computational results (figures

6 and 7) show that a good identification of the $Ni_{60}Al_{35}Pt_5$ parameters has been obtained at the different temperatures considered.

'[Insert Figure 5 about here]'

'[Insert Figure 6 about here]' '[Insert Figure 7 about here]'

3.2.3. Confrontation to experimental data from the literature. During the micro-indentation test, large shear stresses occur, that locally lead to large plastic deformations (beyond 5%). However, the lifetime analysis of thermal barrier coatings is more often performed with the small deformation assumption. It is then particularly important to evaluate the yield stress at 0.2% ($\sigma_{0.2\%}$). But, it is not obvious that the micro-indentation gives pertinent information concerning $\sigma_{0.2\%}$ and a confrontation to data from the literature is necessary.

The mechanical properties of NiAl compounds are highly dependent on the composition of the alloy, in particular the aluminium content (the composition domain extends from 35% to 57% Al in the binary Ni-Al system), the temperature and the strain rate. We have considered experimental data from the literature obtained with conventional characterization methods for a strain rate of around 10^{-4} s^{-1} ([25-27]). The iterative optimisation procedure used in this work allows to identify the parameters of the constitutive equation of the indented material. This constitutive model can then be used to simulate different types of experimental tests, in particular the uniaxial tensile test from which the yield stress at 0.2% can be obtained. In figure 8, the experimental data obtained by Pascoe et al. [27] on a $Ni_{47}Al_{53}$ material are compared with our calculated $\sigma_{0.2\%}$ for a material having the same composition. It is difficult to estimate the errors on these values, as the experimental dispersion on the microindentation data has not been yet included in the optimisation procedure. However, the comparison of calculated properties and experimental data by [27] shows a very good agreement on a large temperature range, which is very encouraging.

The results obtained from microindentation tests on $Ni_{60}Al_{35}Pt_5$ alloy are more difficult to compare with literature data as this alloy is near a phase boundary and apparently, no published data are available corresponding to that aluminium content. It can be seen in figure 9 that the yield stress of this Al-poor material, as derived from microindentation tests is larger than the yield stress of the NiAl materials considered in other studies. These high values are consistent with the fact that the yield stress increases as the aluminium content decreases. It should be also noted that for this particular composition, a martensitic transformation occurs, which can explain the particularly high yield stress values.

'[Insert Figure 8 about here]' '[Insert Figure 9 about here]'

During service, the composition of the bondcoat of a thermal barrier system evolves. Part of its aluminium is consumed by oxidation and due to interdiffusion phenomena with the superalloy substrate, the aluminium and platinum contents vary as a function of time and temperature. In addition, minor elements can diffuse from the substrate. These composition variations are most likely to affect the properties of these NiAl-based bondcoats. Work is now in progress to complete these results to have a complete constitutive behaviour law of these materials as a function of temperature for an extended range of compositions

4. Conclusion

An instrumented microindenter capable of operating up to 1000°C in an inert atmosphere has been developed. The results presented show that it is possible to measure small displacements under an imposed load at high temperature, and to extract a creep law from these measurements for a NiAl(Pt) material. A more complex modelling approach based on FEM calculations, has been developed, which by solving the inverse problem, enables to identify the variables of the constitutive law of NiAl(Pt) materials representative of thermal barrier bondcoats. Confrontation of results obtained with this approach with published data on yield strength show a satisfactory agreement on the large range of temperature explored. Work is under way to complete these results by exploring the whole range of compositions of the NiAl(Pt) domain.

Work remains to be done to determine the limits of the methods (sensitivity analysis, influence of experimental dispersion on the parameters entering the constitutive laws), however, the results obtained thus far indicate that this experimental technique combined with the modelling approach might open up a new way to determine the constitutive behaviour law of materials at a local scale.

Acknowledgements: We thank R. Bouchet for providing the NiAl(Pt) materials, M.-H. Ritti for AFM measurements, C. Babin for some of the microindentation measurements, M. Bejet for his technical contribution to the design, and J.-L. Chaboche for helpful discussions. Part of this study was financially supported by DGA (Délégation Générale à l'Armement).

References

[1] Bhushan Bharat, in *Handbook of Micro/Nano tribology* (1995) p 321-397.
[2] W.C. Oliver, G.M. Pharr, J. Mater. Res. **7** 1564-1583 (1992).
[3] J. Gubicza, Solid State Phenomena **56** 195-200 (1997).
[4] Yan Ping Cao, Jian Lu, Acta Materialia **52** 4023-4032 (2004).
[5] M. Dao, N. Chollacoop, K.J. Van Vliet, T.A. Venkatesh, S. Suresh, Acta Materialia **49** 3899-3918 (2001).
[6] R. Mévrel, La Recherche Aérospatiale **5-6** 381-392 (1996).
[7] C. G. Levi, Current Opinion in Solid State and Materials Science **8** 77-91 (2004).
[8] I.T. Spitsberg, D.R. Mumm, A.G. Evans, Mat. Sci. Engng **A 394** 176-191 (2005).
[9] D. Pan, M.W. Chen, P.K. Wright, K.J. Hemker, Acta Materialia **51** 2205-2217(2003).
[10] J.C.M. Li, Materials Science and Engineering **A322** 23-42 (2002).
[11] T.O. Mulhearn, D. Tabor, J. Inst. Metals **89** 7-12 (1960-61)
[12] A.G. Atkins, A. Silverio, D. Tabor, J. Inst. Metals **94** 369-378 (1966)
[13] P.M. Sargent, M.F. Ashby, Mater. Sci Technol. **8** 594-601 (1992).
[14] M. Fujiwara, M. Otsuka, Mat. Sci. Engng **A319-321** 929-933 (2001).
[15] D. Dorner, K.; K. Röller, B. Skrotzki, B. Stöckhert, G. Eggeler, Mat. Sci. Engng **A357** 346-354 (2003).
[16] H.J. Frost, M.F. Ashby, Deformation-mechanism maps. Pergamon Press (1982)
[17] H. Takagi, M. Fujiwara, K. Kakehi, Mat. Sci. Engng **A387-389** 348-351 (2004).
[18] C.-H. Kim, A.H. Heuer, B.D. Kernan, Ceramic Transactions **156** 107-115 (2004).
[19] B.D. Beake, J.F. Smith, Phil. Mag. A **82**(10) 2179-2186 (2002).
[20] B.D. Beake, S.R. Goodes, J.F. Smith, Z. Metallkde **94** 798-901(2003).
[21] R.D. Noebe, R.R. Bowman, M.V. Nathal, International Materials Review **38**(4) 193–232 (1993).
[22] J.-L. Chaboche, Viscoplastic constitutive equations for the description of cyclic and anisotropic behaviour of metals, Bulletin de l'Académie Polonaise des Sciences, Série Sc. et Techn., **25**, n°1, 33-42 (1977) .
[23] J.-L. Chaboche, Int. J. Plasticity **5**(3) 247-302 (1989).
[24] J. Lemaitre, J.-L. Chaboche, Mechanics of solid materials. Cambridge University Press (1994)
[25] M.J. Lequeux, Influence de l'écart à la stoechiométrie sur la structure et les propriétés mécaniques du composé NiAl, ONERA Publication 1980-3 FR ISSN 0078-379X (1980).

[26] D. Pan, M. W. Chen, P. K. Wright and K. J. Hemker, Acta Materialia **51**(8) 2125-2426 (2003).
[27] R.T. Pascoe and C.W.A. Newey, Metal Science Journal **2** 138-143 (1968).

Table with caption

Table 1. The set of equations of the constitutive model. (Chaboche et al. [22, 23])

$\varepsilon = \varepsilon_e + \varepsilon_p$ (4)	Partition law
$f = J(\sigma - X) - \sigma_y \leq 0$ (5)	Von Mises material $J = \left[\frac{3}{2}(\sigma'_{ij} - X'_{ij})(\sigma'_{ij} - X'_{ij})\right]^{\frac{1}{2}}$ (6)
$X = \sum_{i=1}^{M} X_i = \frac{2}{3}\sum_{i=1}^{M} C_i \alpha_i$ (7)	Kinematical hardening $\dot{\alpha}_i = \dot{\varepsilon}_p - D_i \alpha_i \dot{p}$ (8)
$\dot{\varepsilon}_p = \dot{p}\frac{3}{2}\frac{\sigma' - X'}{\|\sigma - X\|}$ (9)	Viscoplastic Flow $\dot{p} = \|\dot{\varepsilon}_p\| = \left(\frac{2}{3}\dot{\varepsilon}_p : \dot{\varepsilon}_p\right)^{1/2} = \eta_0 \left\langle \frac{f}{\sigma_d} \right\rangle^n$ (10)

Figure captions

Figure 1. Instrumented microindentation equipment for experiments up to 1000°C.

Figure 2. Load-penetration curves for instrumented microindentation on $Ni_{40}Al_{45}Pt_{15}$ with holding the maximum load during 1600s.

Figure 3. Displacement as a function of time for the $Ni_{40}Al_{45}Pt_{15}$ alloy tested by instrumented microindentation (Maximum load: 0.7N, held at the indicated temperature). The continuous lines correspond to the equations in the text (steady-state regime).

Figure 4. Variations of B parameter (see eq. (3) in text) as a function of the inverse of temperature T(K).

Figure 5. Experimental (left) versus computational (right) responses of a NiAlPt material system under load cycling.

Figure 6. Creep indentation tests and simulation at 800°C on a NiAl(Pt) material system validated with the profile of the hardness test marks obtained by AFM.

Figure 7. Experimental versus computational indentation depth at the beginning of dwell time of indentation tests performed at two loading rates.

Figure 8. Comparison of the 0.2% yield stress (strain rate of around 10^{-4} s^{-1}) derived from stress-strain curve calculated from the constitutive law (whose parameters were identified from the microindentation data) on $Ni_{47}Al_{53}$ compound with experimental values by Pascoe and Newey [27].

Figure 9. Comparison of the 0.2% yield stress (strain rate of around 10^{-4} s^{-1}) derived from stress-strain curve calculated from the constitutive law (whose parameters were identified from the microindentation data) on $Ni_{60}Al_{35}Pt_5$ compound with experimental values from Lequeux [25], Hemker and coll. [26], and Pascoe and Newey [27] for various NiAl compounds.

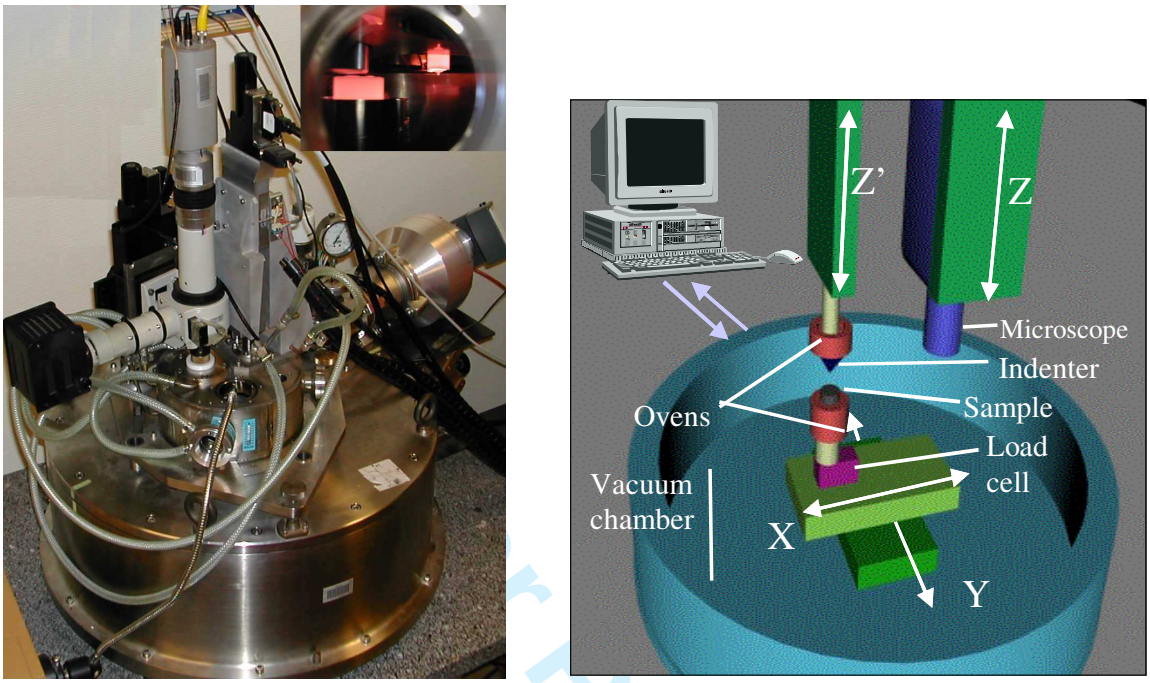

Figure 1. Instrumented microindentation equipment for experiments up to 1000°C.

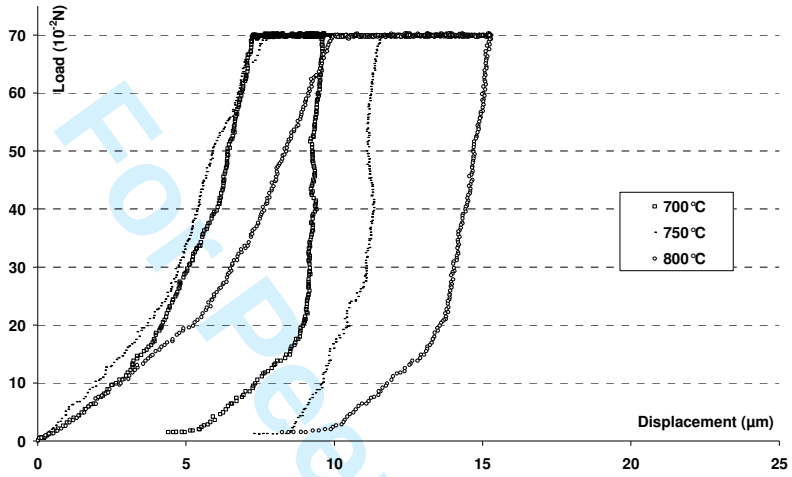

Figure 2. Load-penetration curves for instrumented microindentation on $Ni_{40}Al_{45}Pt_{15}$ with holding the maximum load during 1600s.

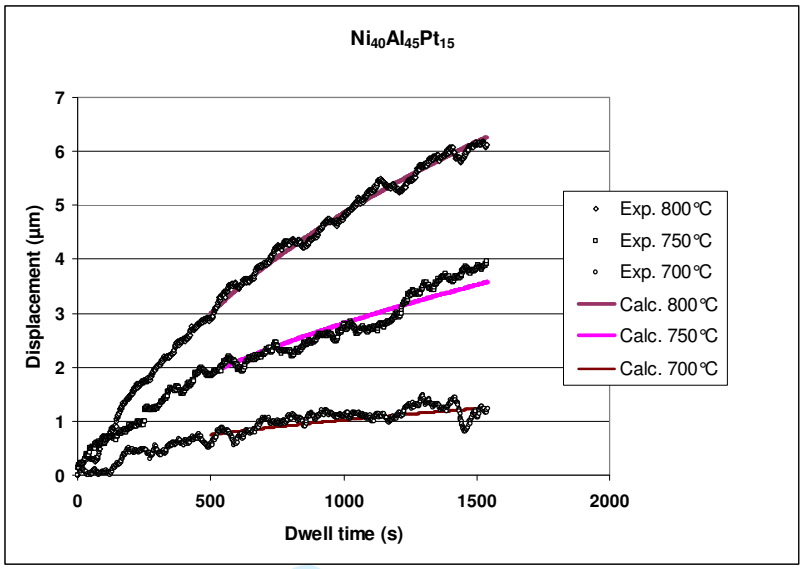

Figure 3. Displacement as a function of time for the $Ni_{40}Al_{45}Pt_{15}$ alloy tested by instrumented microindentation (Maximum load: 0.7N, held at the indicated temperature). The continuous lines correspond to the equations in the text (steady-state regime).

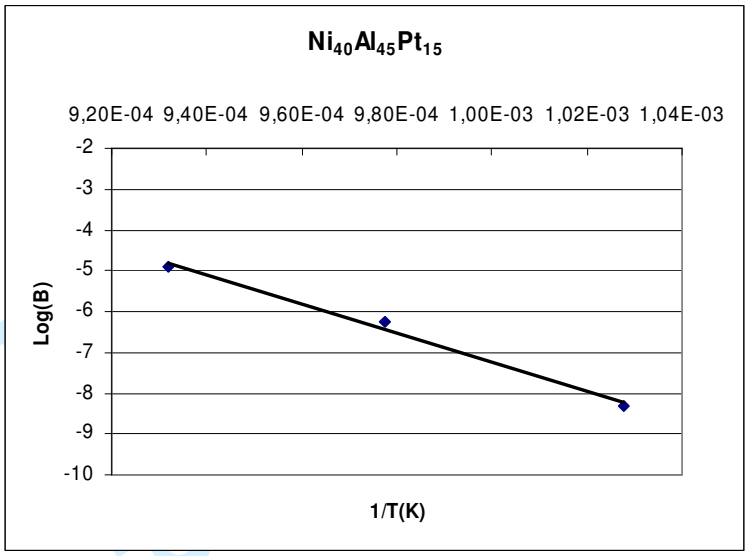

Figure 4. Variations of B parameter (see eq. (3) in text) as a function of the inverse of temperature T(K).

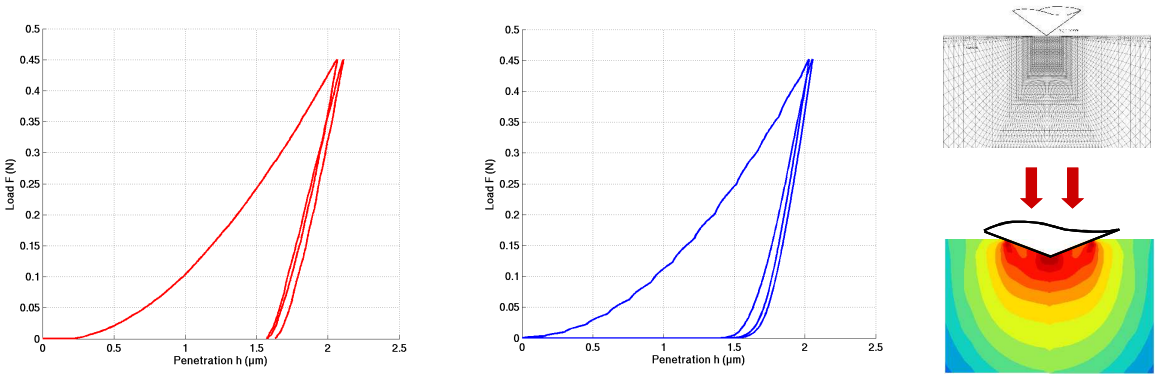

Figure 5. Experimental (left) versus computational (right) responses of a NiAl(Pt) material system under load cycling.

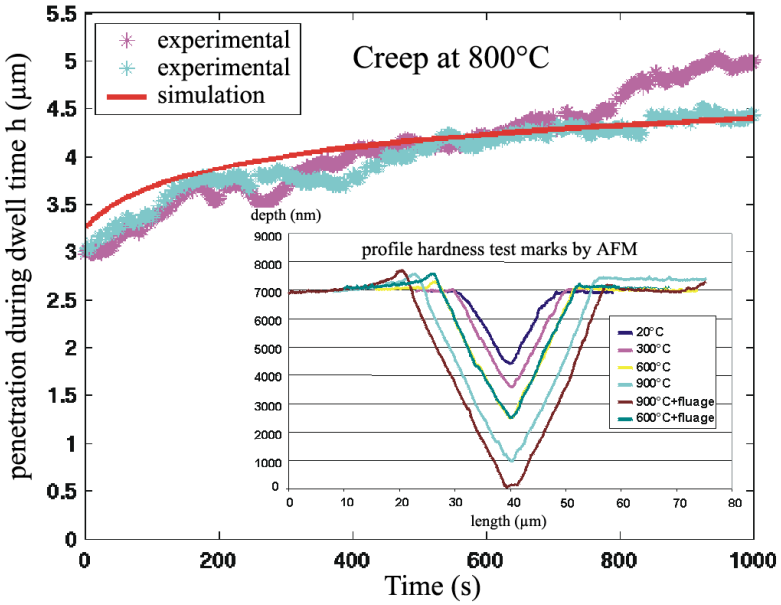

Figure 6. Creep indentation tests and simulation at 800°C on a NiAl(Pt) material system validated with the profile of the hardness test marks obtained by AFM.

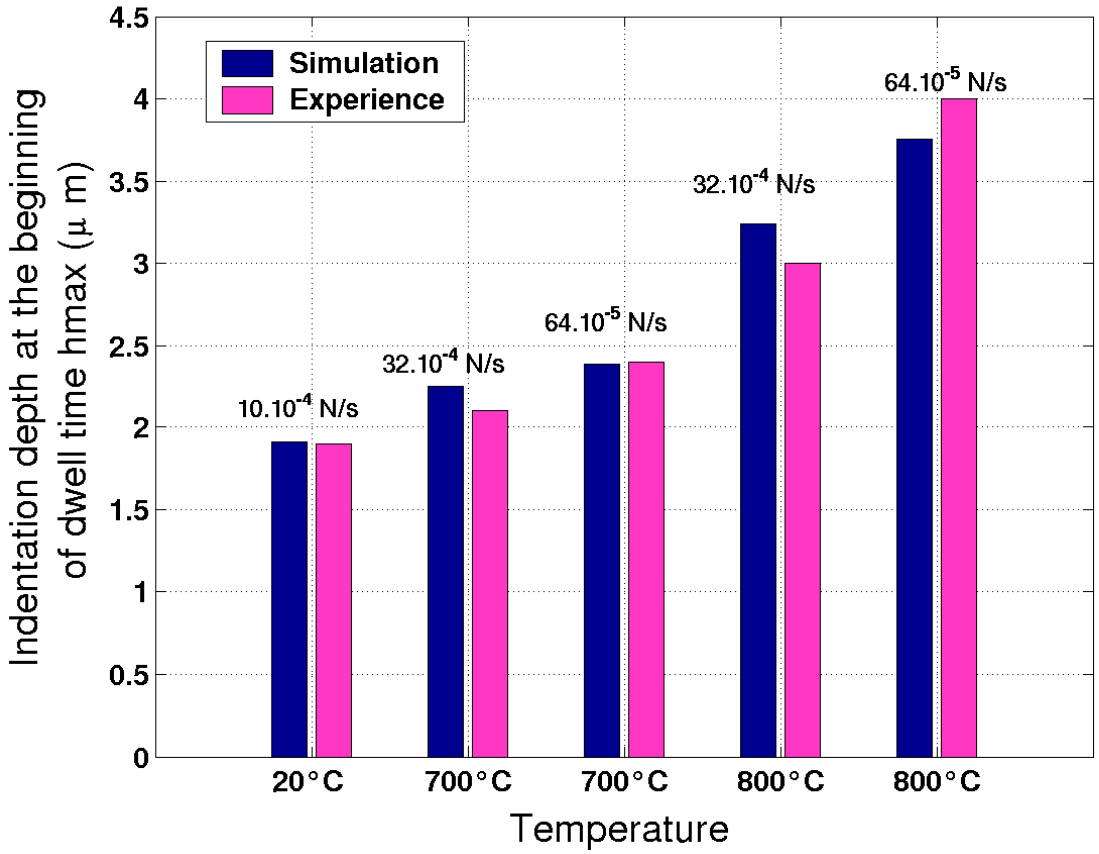

Figure 7. Experimental versus computational indentation depth at the beginning of dwell time of indentation tests performed at two loading rates.

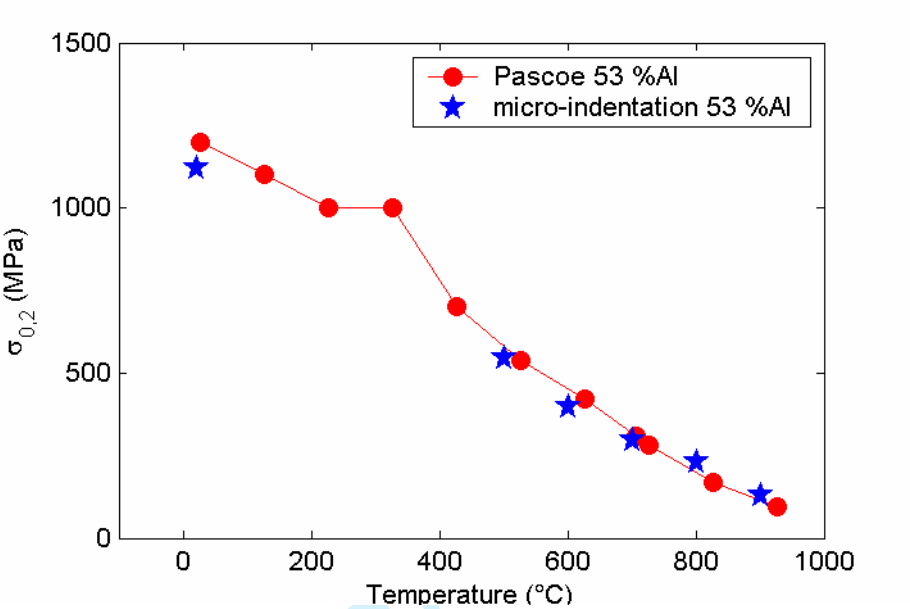

Figure 8. Comparison of the 0.2% yield stress (strain rate of around 10^{-4} s^{-1}) derived from stress-strain curve calculated from the constitutive law (whose parameters were identified from the microindentation data) on $Ni_{47}Al_{53}$ compound with experimental values by Pascoe and Newey [27].

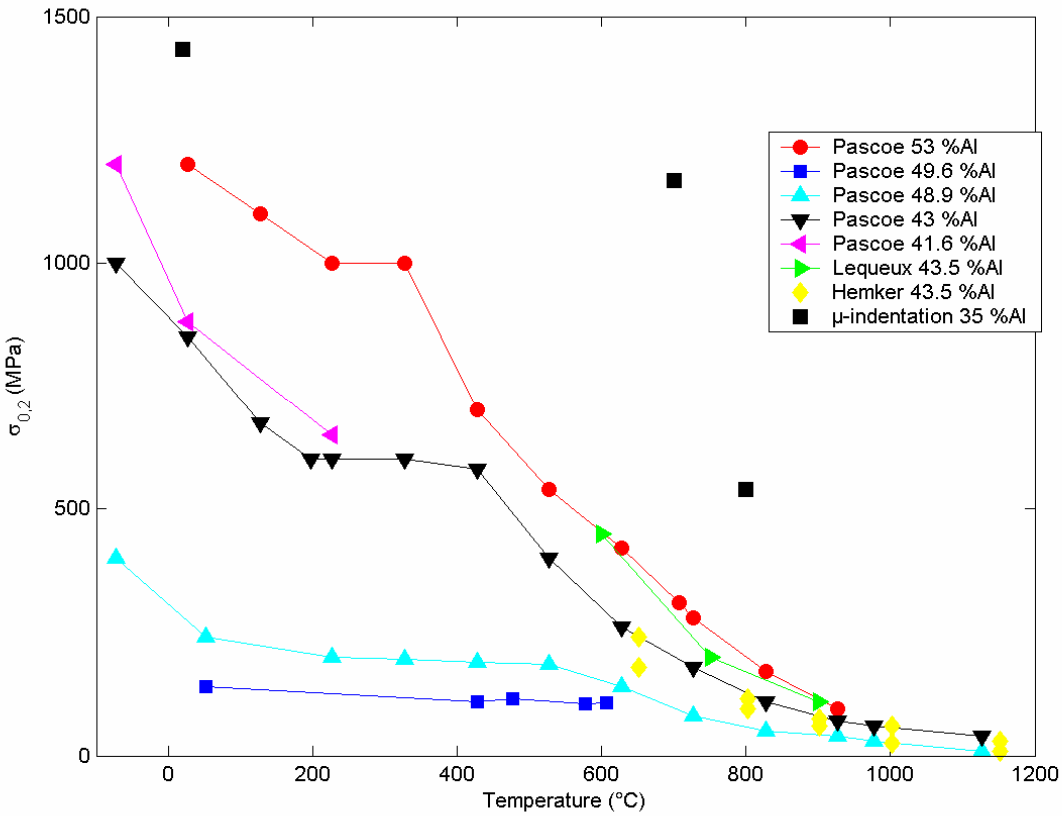

Figure 9. Comparison of the 0.2% yield stress (strain rate of around 10^{-4} s^{-1}) derived from stress-strain curve calculated from the constitutive law (whose parameters were identified from the microindentation data) on $Ni_{60}Al_{35}Pt_5$ compound with experimental values from Lequeux [25], Hemker and coll. [26], and Pascoe and Newey [27] for various NiAl compounds.